

Supplyment Material

Manipulating Key Intermediates and Suppressing Hydrogen Evolution Reaction via Dual Roles of Bi for High-Efficiency Nitrate to Ammonia and Energy Conversion

Chunming Yang^{a,b,*}, Tingting Wei^a, Chuantao Wang^{a,*}, Feng Yue^a, Xiang Li^a, Huijuan Pang^a, Xueyan Zheng^a, Yantu Zhang^{a,*}, Feng Fu^{a,*}

^a Shaanxi Key Laboratory of Chemical Reaction Engineering, College of Chemistry & Chemical Engineering, Yan'an University, Yan'an 716000, Shaanxi, China

^b Hubei Three Gorges Laboratory, Yichang 443007, Hubei, China

*Corresponding author:

E-mail: chunmingyang@yau.edu.cn (C. Yang), chuantaowang@yau.edu.cn (C. Wang), zhyt1969@163.com (Y. Zhang), yadxfufeng@126.com (F. Fu)

Experimental Section

1. Ion concentration detection methods

UV-Vis spectrophotometer was used to detect the ion concentration of pre-test and post-test electrolytes after dilution to appropriate concentration. The specific detection methods are as follows:

Detection of NO_3^- -N: 100 μL electrolyte is extracted from the cathode compartment and diluted to 3 mL, 100 μL 0.8 wt% sulfamic acid solution is added above diluted electrolyte and left for 15 min. The absorption spectra of the above mixed solutions are determined in the wavelength range of 190-300 nm using UV-Vis spectrophotometry. The calibration curve was attained via a series of standard KNO_3 solutions.

Detection of NO_2^- -N: For preparing the color reagent, p-aminobenzenesulfonamide (20 g), N-(1-Naphthyl) ethylenediamine dihydrochloride (1 g) are dissolved in a mixture containing phosphoric acid (50 mL) and deionized water (500 mL). 100 μL electrolyte is added above diluted electrolyte and left for 15 min. The absorption intensity of NO_2^- -N at 540 nm was measured by UV-Vis spectrophotometry. The calibration curve was attained via a series of standard KNO_2 solutions.

Detection of NH_4^+ -N: The concentration of NH_4^+ is conducted with Nessler's reagent as coloring agent. 100 μL electrolyte after NO_3RR is taken out from the cathodic compartment and diluted to 3 mL. 100 μL Nessler's reagent and 100 μL sodium potassium tartrate solution (500 g L^{-1}) are added to the above diluted solution. After being left standing for 15 min, the absorbance at 420 nm is measured by UV-Vis spectroscopy. The calibration curve is attained via a series of standard NH_4Cl solutions. The NH_3 was further qualitatively detected by $^1\text{H-NMR}$ spectroscopy. Hydrogen NMR spectra are obtained by 64 scans using water suppression method. Typically, 400 μL electrolyte is mixed with 300 μL DI water and 300 μL 2M HCl. Then, 500 μL above solution is mixed with 100 μL internal standard solution (50 ppm m/m dimethyl sulfoxide dissolved in D_2O) for nuclear magnetic detection.

Detection of N_2H_4 -N: A mixture of 4 g 4-(Dimethylamino) benzaldehyde, 1 M hydrochloric acid (20 mL) and ethanol (200 mL) was used as a color developing agent.

Dilute a certain amount of electrolyte to 4 ml with a pH value close to 7. Add 200 μ L color developer to the above solution and mix well. The absorption intensity of N₂H₄-N at 457 nm was measured by UV-Vis spectroscopy.

2. Calculation of the yield and FE

The yield of NH₃ was calculated using :

$$\text{Yield (NH}_3\text{)} = (C_{\text{NH}_3} \times V) / (M_{\text{NH}_3} \times t \times m)$$

The FE was calculated using :

$$\text{Faradaic efficiency} = (8F \times C_{\text{NH}_3} \times V) / (M_{\text{NH}_3} \times Q) \times 100\%$$

Where C_{NH_3} and $C_{\text{NO}_2^-}$ are the concentration of NH₃ and NO₂⁻, V is the electrolyte volume, t is the electrolysis time, m is the mass of catalyst, F is the Faradaic constant (96485 C mol⁻¹), Q is the total charge passing the electrode.

3. Calculation of turnover frequency (TOF)

The value can be obtained according to the equation:

$$\text{TOF} = \frac{J}{8n * F}$$

Where J is the current density during NO₃RR in 0.1M KNO₃+0.1M KOH solution, 8 represents the stoichiometric number of electrons consumed in NO₃RR, n is the number of active sites, F is the Faraday constant (~96485 C/mol). The charge Q of surface active sites (n) can be described by $Q = nF$, therefore, we can evaluate the upper limit of the active site number (n) according to the follow formula:

$$n = \frac{Q}{F}$$

Here F and Q correspond to the Faraday constant and the whole charge of CV curve, respectively. Thus, the TOF can be calculated by this equation:

$$\text{TOF} = \frac{J}{\frac{Q}{F} * F} = \frac{J}{8Q}$$

And the Q can be calculated based on the equation:

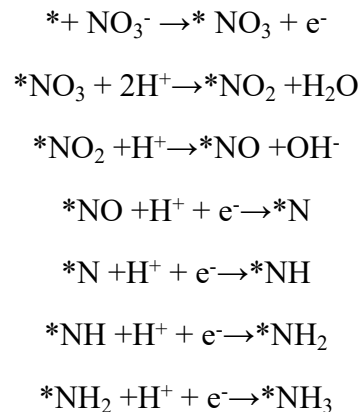
$$Q = \frac{S}{2v}$$

Where v is the scan rate (50 mV/s in this work), and S is the integrated areas of CV curves. Finally, the TOF can be obtained by this equation:

$$TOF = \frac{Jv}{S}$$

4. Theoretical simulation

All calculations in this work were performed using the Vienna ab initio simulation package (VASP) based on the density functional theory (DFT). The projected augmented wave (PAW) method with PBE functional was employed for the generation of pseudopotential. The kinetic energy cutoff for the plane-wave expansion was set to 400 eV. All the structural models were fully relaxed to the ground state with the convergence of energy and forces setting to 10^{-5} eV and 0.01 eV \AA^{-1} , respectively. Bi-CoS₂ (200) surface was chosen for DFT calculations. One surface Co was removed to model the Bi-CoS₂ surface. Here, the chemical reaction considered can be summarized with the reaction equations below.



Where $*$ represents the active site. Then, the reaction free energy change can be obtained with the equation below:

$$\Delta G = \Delta E + \Delta \text{EZPE} - T\Delta S$$

Where ΔE is the total energy difference before and after intermediate adsorbed, ΔEZPE and ΔS are, respectively, the differences of ZPE zero point energy and entropy. The zero point energy and entropy of free molecules and adsorbents were obtained from the vibrational frequency calculations. To describe the charged NO_3^- species as

reference, the neutral HNO_3 gas phase was chosen as reference and then the energy of nitrate ion was obtained from the thermodynamic cycle to avoid the difficulty of using periodic DFT reference and then the energy of calculations for charged systems.

5. Assembly of the Zn-NO_3^- battery and electrochemical test

For testing in Zn-NO_3^- battery, Bi- CoS_2 and Zn sheet were placed on both sides of an anion exchange membrane as the cathode and anode respectively, where 1 M KOH +0.1 M KNO_3 as the catholyte and 1 M KOH as the anolyte. The discharging polarization curves with a scan rate of 5 mV/s and galvanostatic tests were conducted using a CHI 760E workstation and Land 2001A battery test system at room temperature, respectively. After electrochemical test, the electrolyte was diluted for the next detection. The power density (P) of zinc-nitrate battery was determined by $P = I \times V$, where I and V are the discharge current density and voltage, respectively.

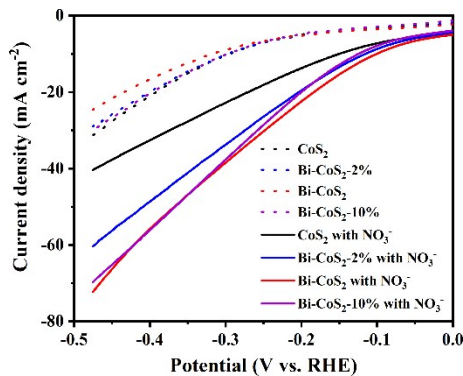


Fig. S1. LSV curves of the Bi- CoS_2 - $x\%$ ($x=0, 2, 6, 10$) with and without NO_3^- .

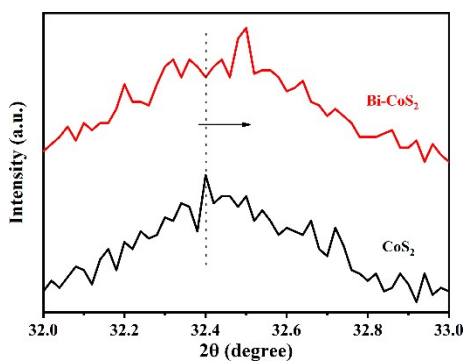


Fig. S2. Magnified view of the XRD patterns for CoS_2 and Bi- CoS_2 .

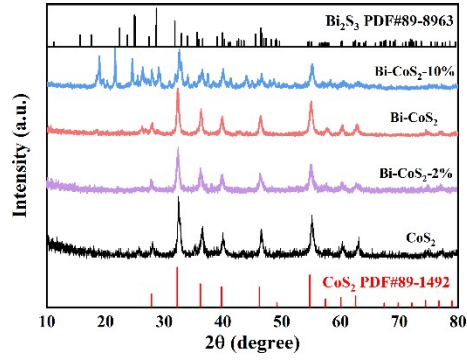


Fig. S3. XRD pattern of Bi-CoS₂-x% (x=0, 2, 6 10).

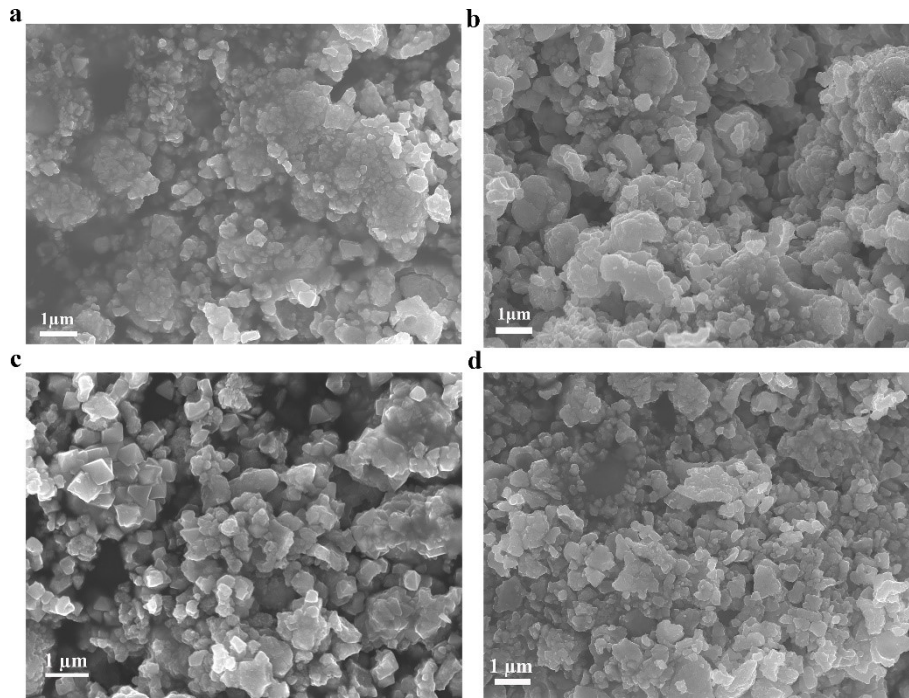


Fig. S4. SEM image of (a) CoS₂, (b) Bi-CoS₂-2%, (c) Bi-CoS₂-6% (Bi-CoS₂) and (d) Bi-CoS₂-

10%.

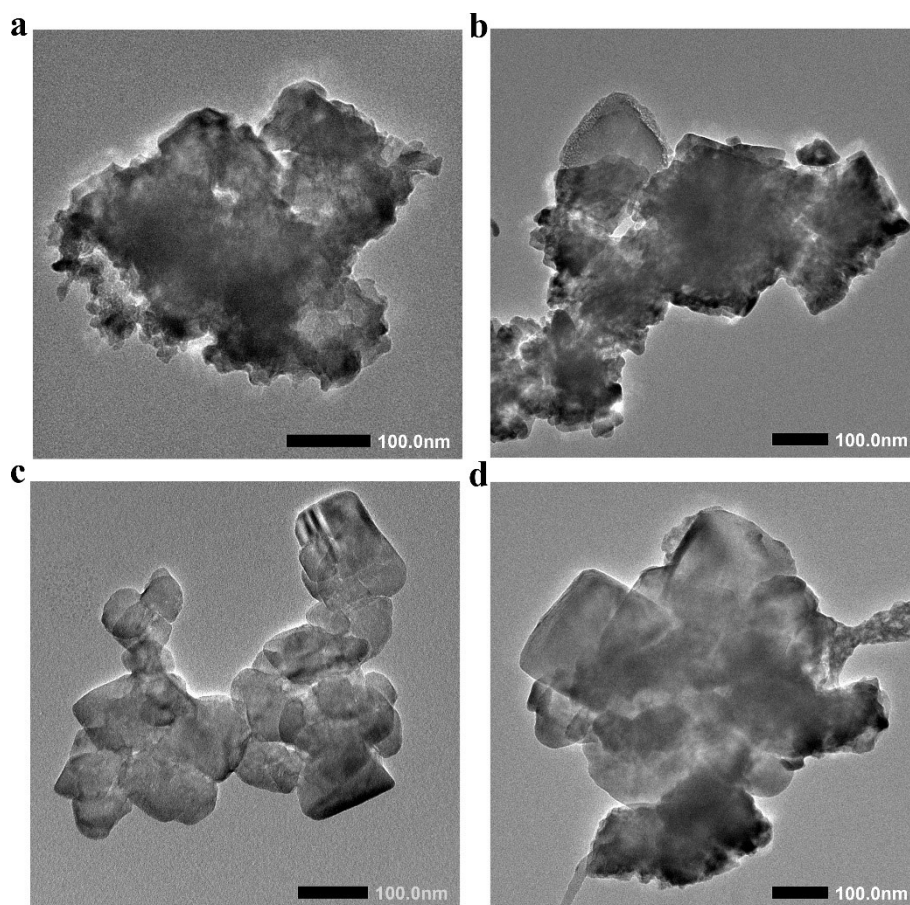


Fig. S5. HRTEM image of (a) CoS₂, (b) Bi-CoS₂-2%, (c) Bi-CoS₂-6% (Bi-CoS₂) and (d)Bi-CoS₂-10%.

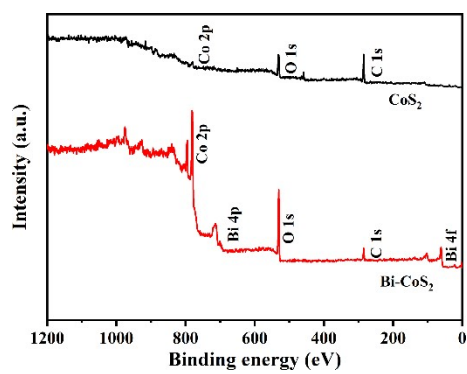


Fig. S6. XPS survey spectra of CoS₂ and Bi-CoS₂.

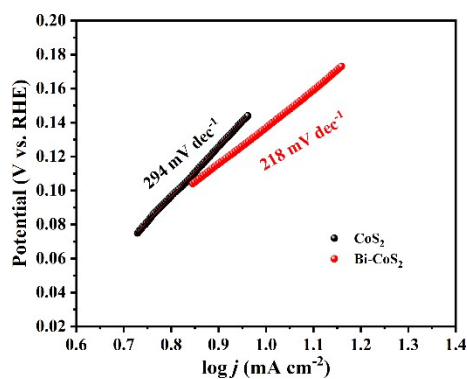


Fig. S7. Tafel slopes of CoS₂ and Bi-CoS₂.

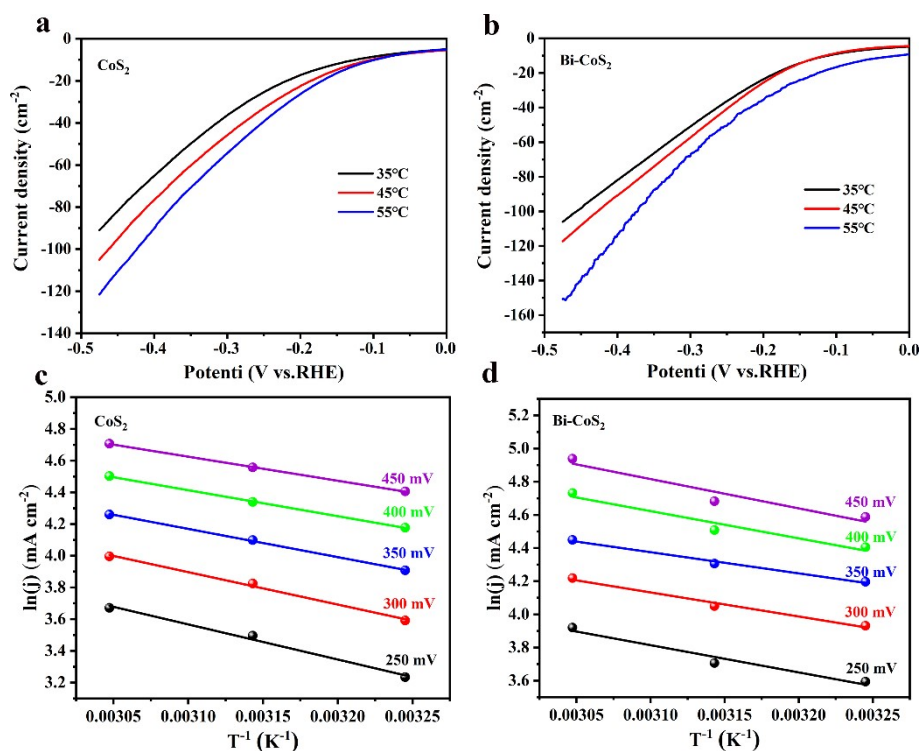


Fig. S8. Polarization curves of (a) CoS₂ and (b) Bi-CoS₂ at different temperatures. Arrhenius plots of (c) CoS₂ and (d) Bi-CoS₂.

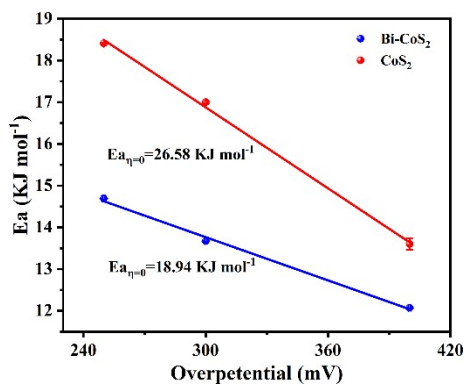


Fig. S9. Activation energy (E_a) of CoS₂ and Bi-CoS₂ obtained through trend extrapolation.

Polarization curves at different temperatures for the catalysts were collected to assess the apparent

electrochemical E_a for NO_3RR using the Arrhenius relationship, $\frac{\partial \log_{10}(i_0)}{\partial \frac{1}{T}} = -\frac{E_a}{2.3R}$, where i_0 is the exchange current density, T is the temperature, and R is the universal gas constant. The derived Arrhenius plots were fitted at different overpotentials and the apparent electrochemical E_a could be figured out from the slope of curves. Polarization curves at different temperatures and Arrhenius plots of CoS_2 , Bi-CoS_2 were shown in Supplementary Figure 9, which are used for further activation energy (E_a) calculation.

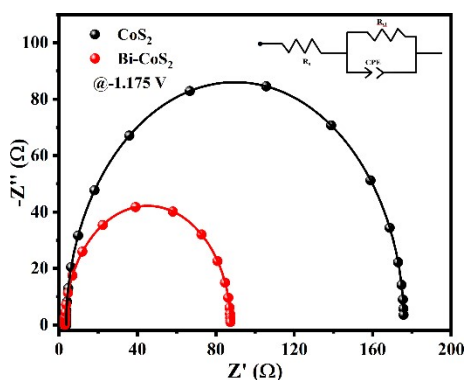


Fig. S10. Nyquist plots of CoS_2 and Bi-CoS_2 .

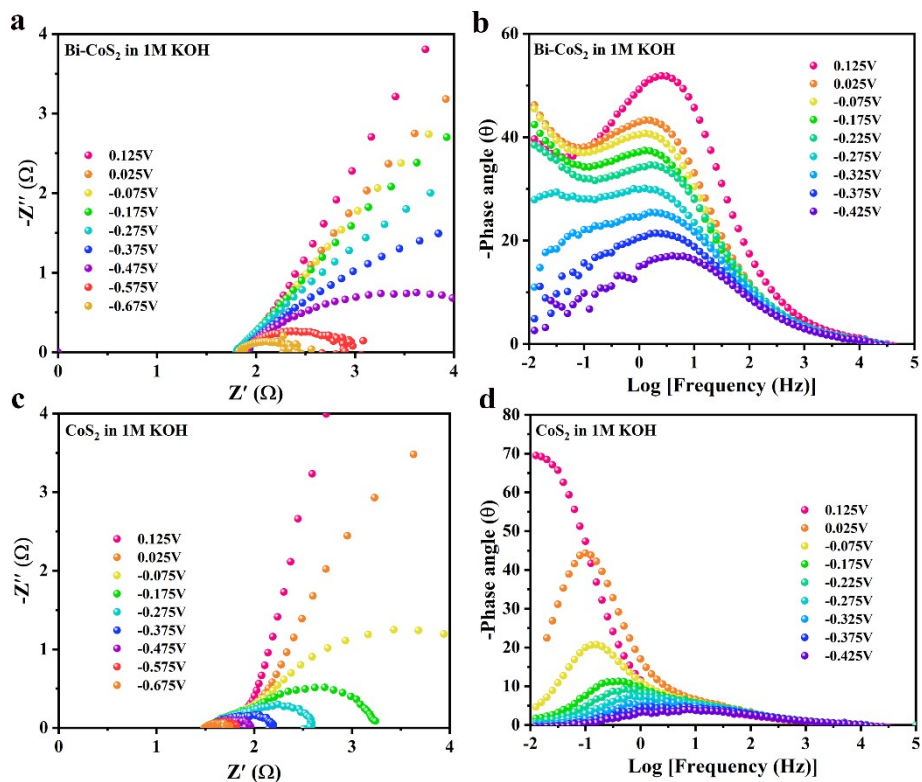


Fig. S11. Nyquist plots and bode phase plots for Bi-CoS₂ and CoS₂ in 1 M KOH.

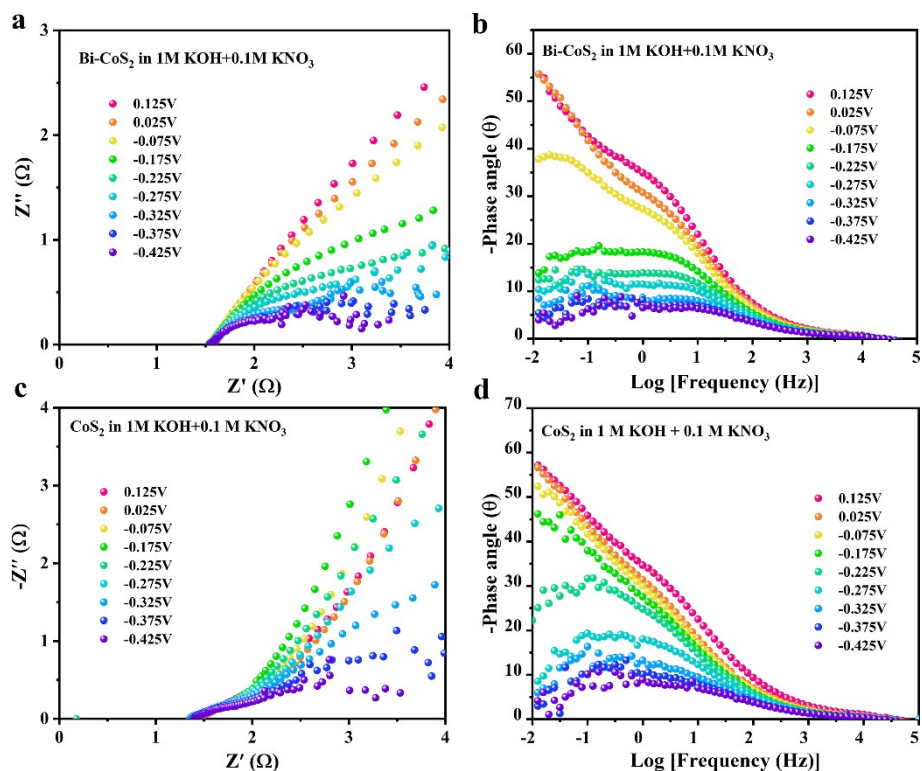


Fig. S12. Nyquist plots and bode phase plots for Bi-CoS₂ and CoS₂ in 1 M KOH + 0.1 M KNO₃.

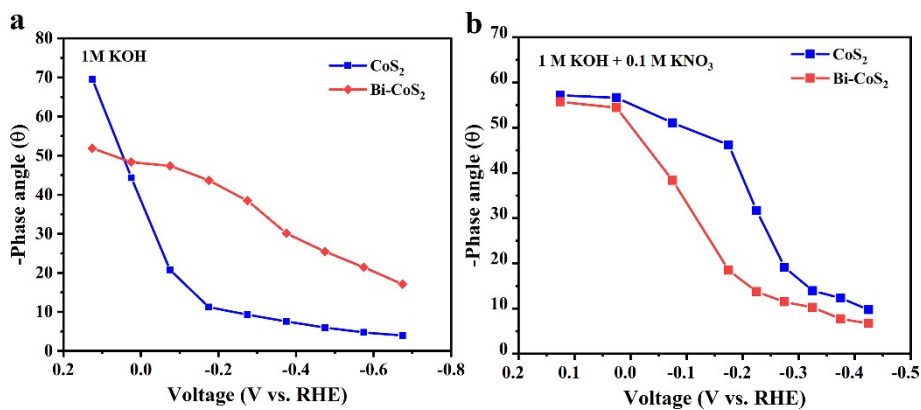


Fig. S13. Response of phase angle to applied potential.

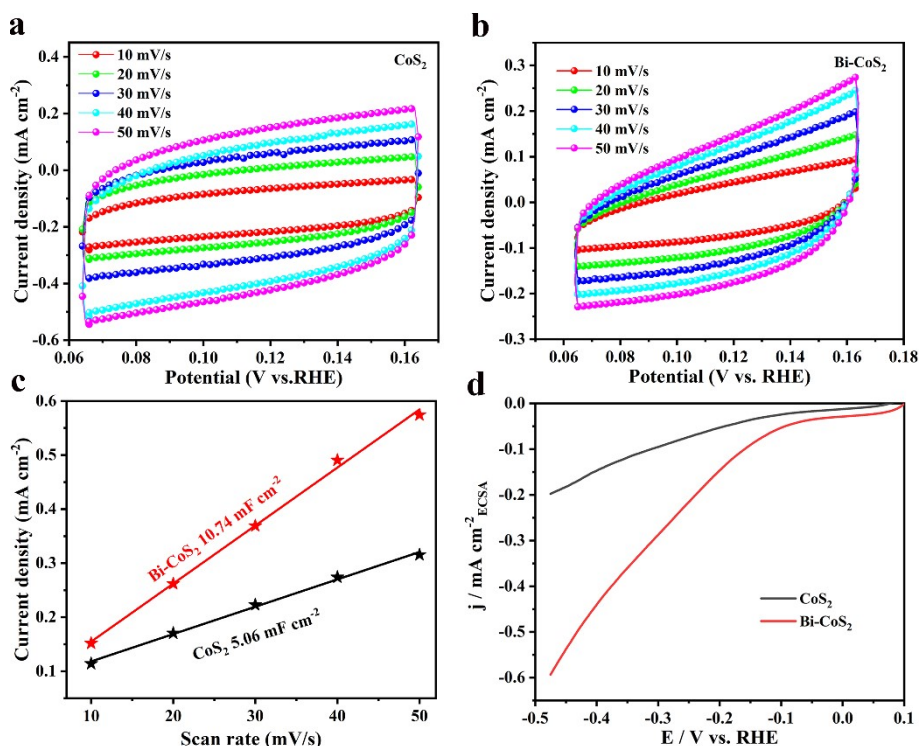


Fig. S14. Cyclic voltammetry profiles obtained on the (a) CoS_2 and (b) Bi-CoS_2 at the sweep rates of 10, 20, 30, 40, 50 and 100 mV s^{-1} . (c) Plots of the current density versus the scan rate for CoS_2 and Bi-CoS_2 . (d) ECSA-normalized LSV curves.

A linear fit determined the specific capacitance to be 10.74 mF cm^{-2} for Bi-CoS_2 and 5.06 mF cm^{-2} for CoS_2 . In the following calculations of electrochemical active surface area, we assumed it as $40 \text{ } \mu\text{F cm}^{-2}$. The ECSAs is then calculated by the following formula:

$$A_{ECSA}^{\text{Bi-CoS}_2} = \frac{10.74 \text{ mF cm}^{-2}}{40 \text{ } \mu\text{F}^{-2} \text{ per cm}_{ECSA}^2} = 268.5 \text{ cm}_{ECSA}^2$$

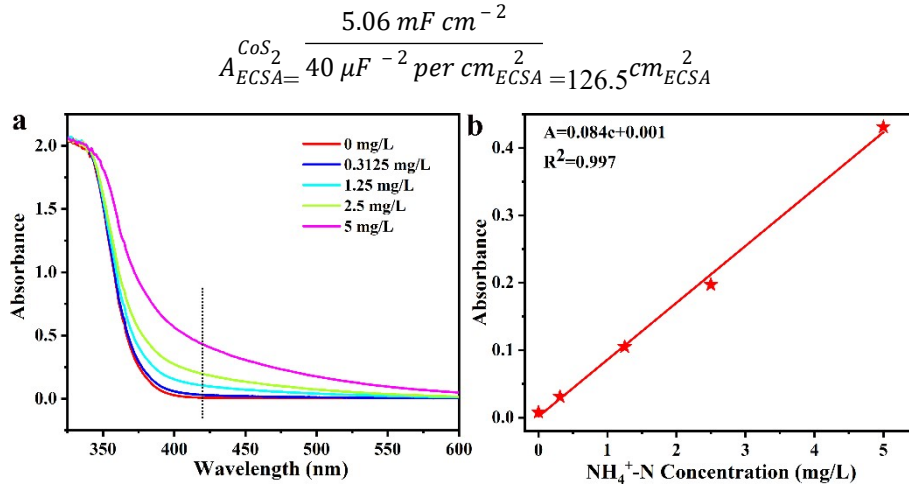


Fig. S15. (a) UV-Vis absorption spectra of NH_4^+ standard solution with different concentrations.

(b) Linear relationship between light absorbance at 420 nm wavelength and the concentration of NH_4^+ standard solution.

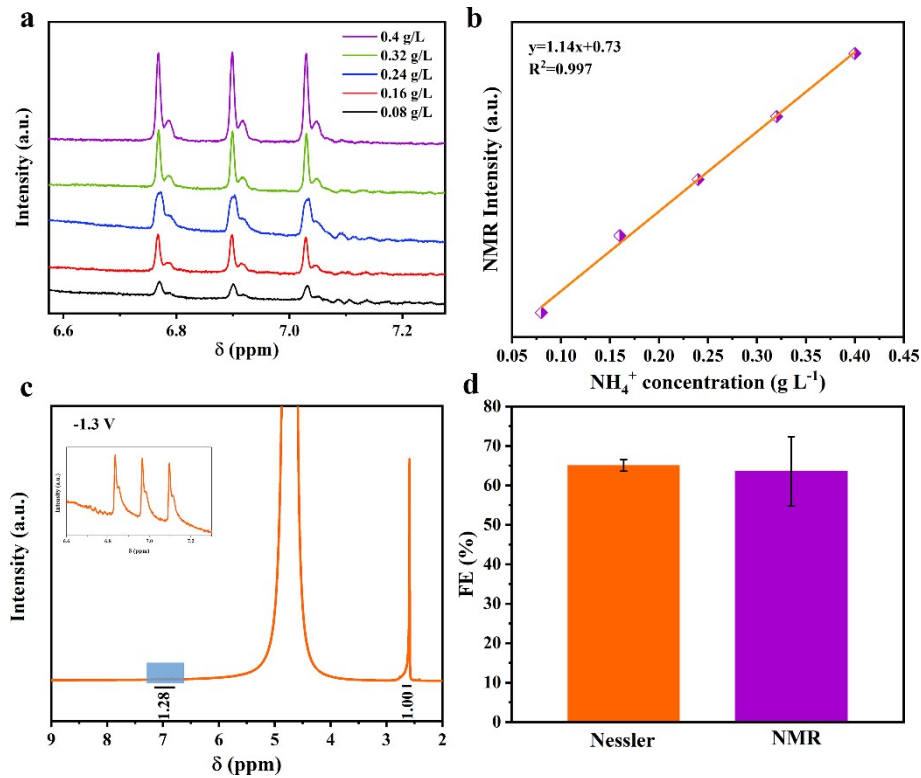


Figure 16. (a) 1H NMR spectra for the standard NH_4^+ solution samples and (b) the corresponding calibration curve. (c) 1H NMR spectrum for the obtained electrolyte as applied the voltage of -1.3 V, and (d) the ammonia FEs comparison between Nessler method and NMR.

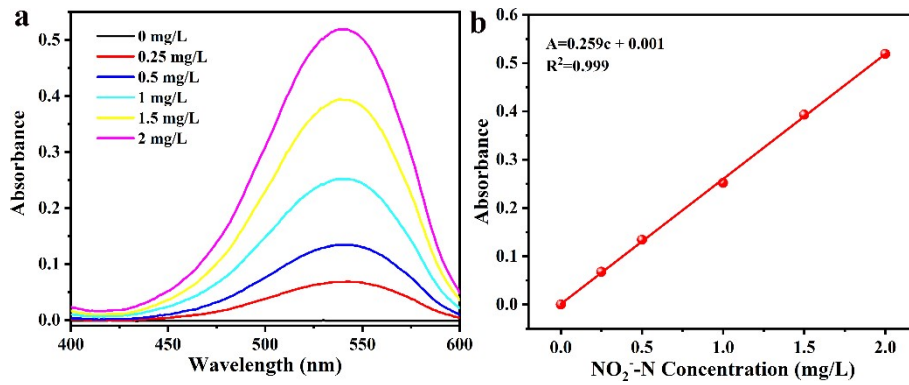


Fig. S17. (a) UV-Vis absorption spectra of NO_2^- standard solution with different concentrations.

(b) Linear relationship between light absorbance at 540 nm wavelength and the concentration of NO_2^- standard solution.

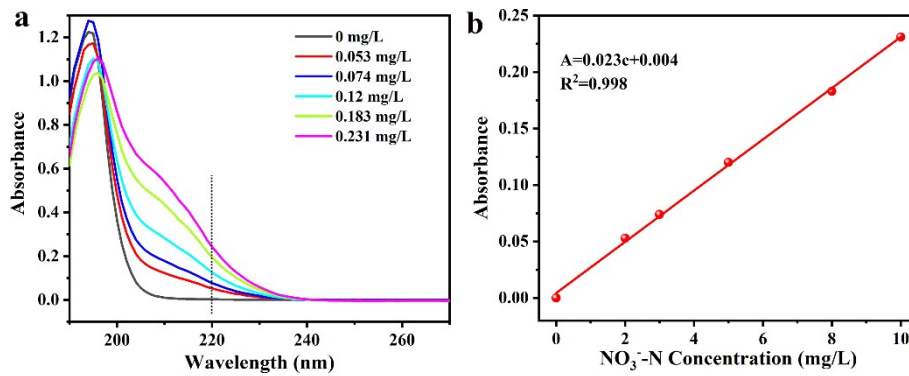


Fig. S18. (a) UV-Vis absorption spectra of NO_3^- standard solution with different concentrations.

(b) Linear relationship between light absorbance at 220 nm wavelength and the concentration of NO_3^- standard solution.

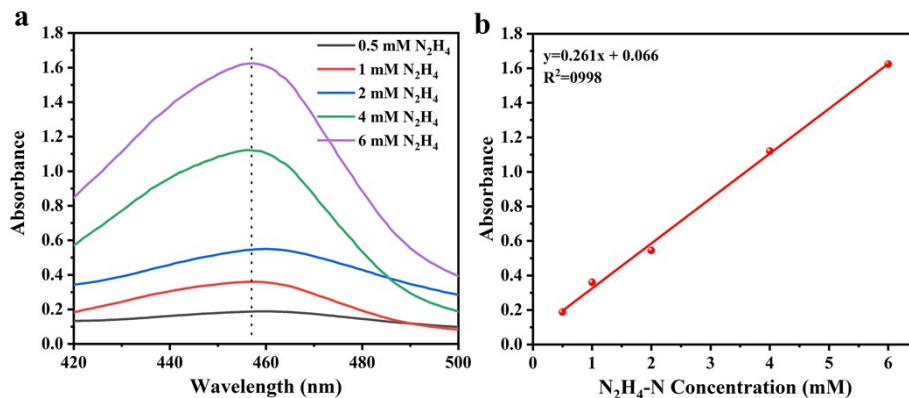


Fig. S19. (a) UV-Vis absorption spectra of N_2H_4 standard solution with different concentrations.

(b) Linear relationship between light absorbance at 457 nm wavelength and the concentration of N_2H_4 standard solution.

N₂H₄ standard solution.

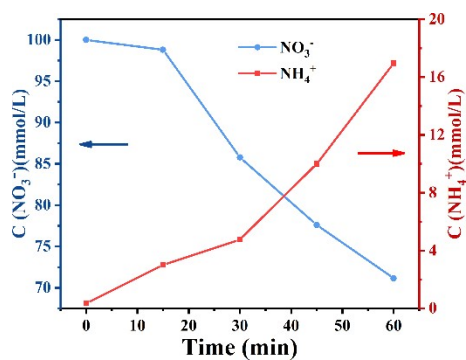


Fig. S20. Time-dependent concentration change of NO₃⁻ and ammonia (NH₄⁺) over Bi-CoS₂ at -

0.2 V vs. RHE.

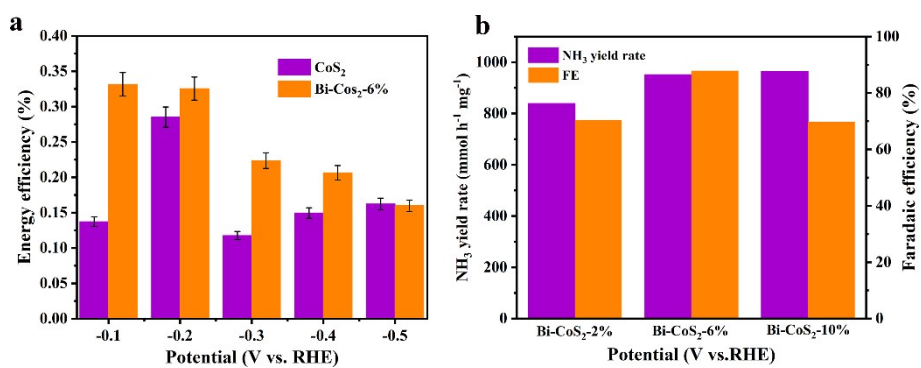


Fig. S21. (a) EE of NO₃RR for CoS₂ and Bi-CoS₂. (b) NH₃ yield rate and NH₃ FE of NO₃RR for

different samples at 0.2 V vs. RHE.

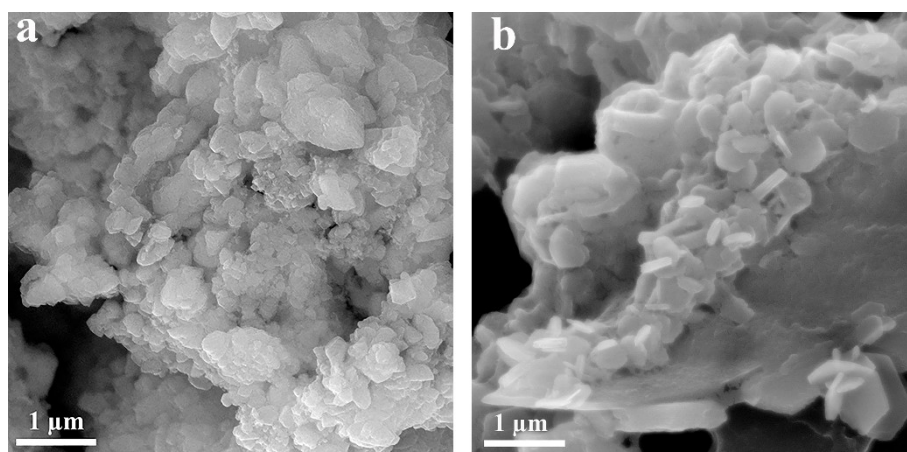


Fig. S22. SEM of Bi-CoS₂ (a) before and (b) after the durability test.

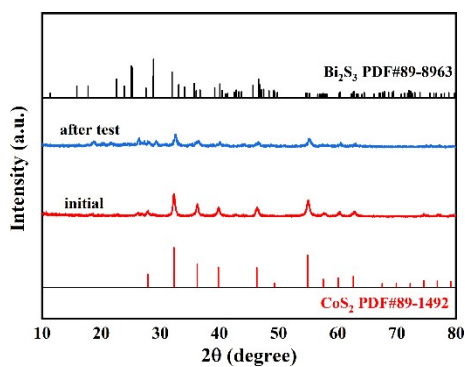


Fig. S23. XRD of Bi-CoS₂ before and after the electrochemical test.

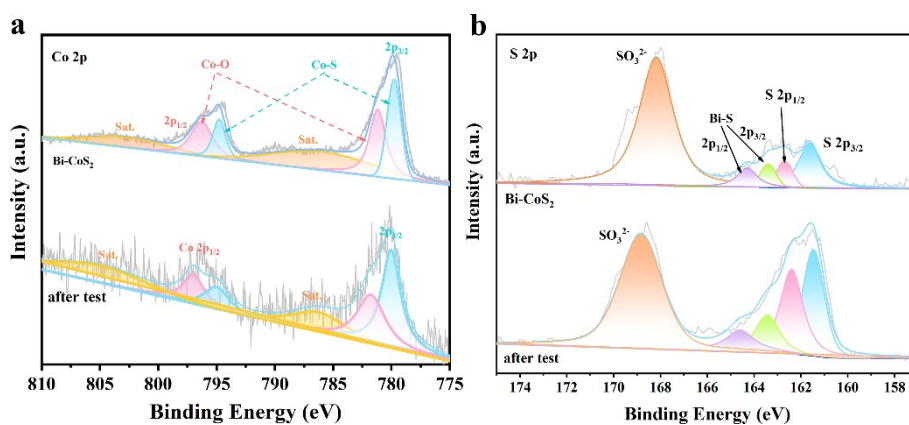


Fig. S24. XPS before and after the durability test.

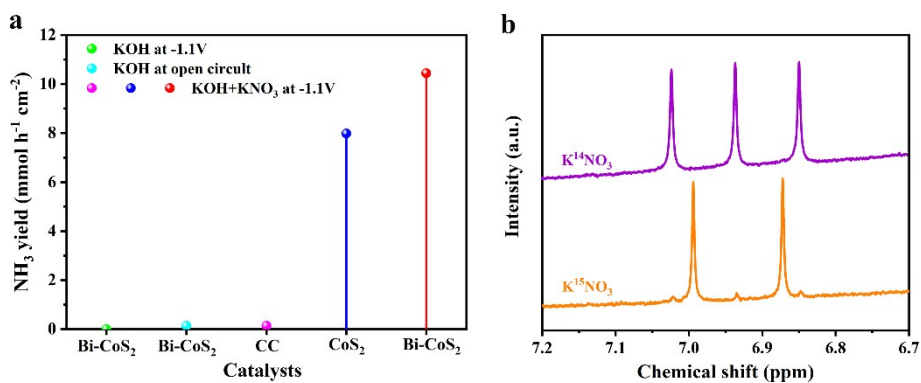


Fig. S25. (a) Control experiment results and (b) ¹H NMR spectra of the electrolyte after NO₃RR

using ¹⁵NO₃⁻ and ¹⁴NO₃⁻ as the nitrogen source, respectively.

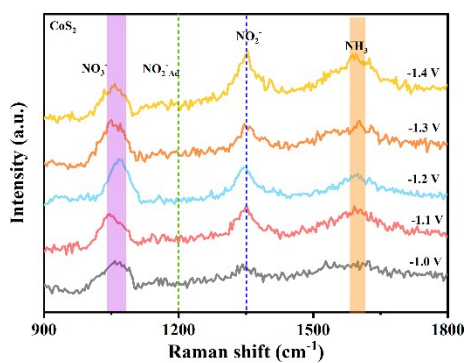


Fig. S26. In-situ Raman spectra of CoS_2 .

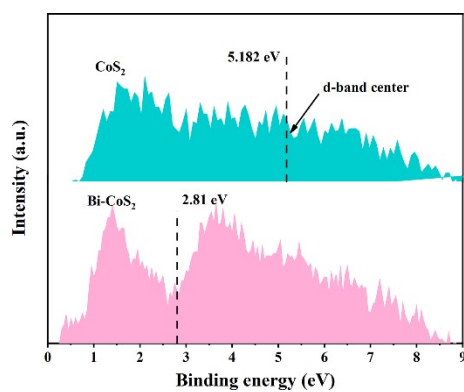


Fig. S27. XPS surface valence band spectra of CoS_2 and Bi-CoS_2 .

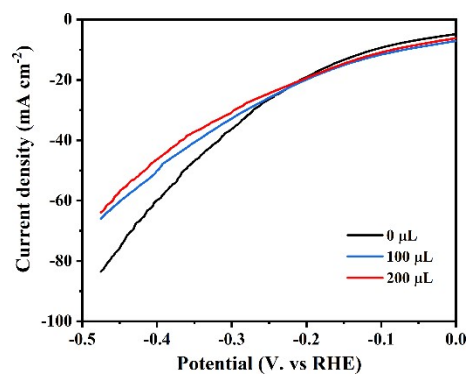


Fig. S28. LSV curves of Bi-CoS_2 in 0.1 M KOH + 0.1 M KNO_3 electrolyte without and with TBA.

Table S1. Element contents of obtained electrocatalysts tested by ICP-OES.

Catalysts	Bi (%)	Co (%)	S (%)
CoS ₂	0	41.87	54.91
Bi-CoS ₂ -6% (Bi-CoS ₂)	8.93	38.60	50.31
Bi-CoS ₂ -2%	3.40	44.24	52.01
Bi-CoS ₂ -10%	14.16	35.14	49.97

Table S2. Detailed process of TOF calculation.

Sample	Voltage (mV)	J (A)	v (mV/s)	S (cm ²)	TOF (s ⁻¹)
Bi-CoS ₂	50	0.006605	50	0.02413	1.3686×10 ⁻²
CoS ₂	50	0.005926	50	0.053685	0.5519×10 ⁻²

Table S3. Comparison of NH₃ synthesis performance between NO₃RR electrocatalyst and Bi-CoS₂.

Catalysts	NH ₃ FE (%)	NH ₃ Yield (μg·cm ⁻² ·h ⁻¹)	Ref.
MoS ₂ /GF	76.6	1690	1
Fe-SnS ₂	85.6	7200	2
Cu _{2-x} S/MoS ₂	84.5	3026	3
Fe/Cu HNG	92.51	18360	4
Fe-N/P-C	90.3	17980	5
FeS ₂ @TiO ₂	85.4	14671	6
Bi ₂ S ₃ /MoS ₂	88.4	2556.8	7
FeS ₂ /RGO	83.7	2320	8
Cu ₂ S/CuO	88.6	6630	9
CoS ₂	77.22	2925.5	This work
Bi-CoS ₂	87.18	5907.7	This work

Table S4. Comparison of Zn-NO₃⁻ battery performances for Bi-CoS₂ with other reported catalysts.

Catalyst	FE (%)	NH ₃ Yield (mg·cm ⁻² ·h ⁻¹)	Power density (mW cm ⁻²)	OCV (V)	Ref.
Pd/TiO ₂	81.3	0.54	0.87	0.81	10
C/Co ₃ O ₄	95.1	0.802	6.03	1.45	11
Cu/Cu ₂ O/Pi NWs	87.64	0.695	3.89	1.22	12
0.6W-O-CoP	75.6	2.79	9.27	0.68	13

Fe/NiP	85	0.38	3.25	1.22	¹⁴
Bi-CoS ₂	95.76	16.32	16.3	1.38	This work

Reference

- [1] L. Zhang, J. Liang, Y. Wang, T. Mou, Y. Lin, L. Yue, T. Li, Q. Liu, Y. Luo, N. Li, *Angew. Chem.* 133 (2021) 25467-25472.
- [2] K. Chen, Y. Luo, P. Shen, X. Liu, X. Li, X. Li and K. Chu, *Dalton Transactions*, 2022, 51, 10343-10350.
- [3] T. Jiang, Y. Liu, D. Zhang, Q. Chen, L. Li, N. Liu, C. Zhou, L. Li and B. Mao, *ACS Sustainable Chemistry & Engineering*, 2024, 12, 5979-5990.
- [4] S. Zhang, J. Wu, M. Zheng, X. Jin, Z. Shen, Z. Li, Y. Wang, Q. Wang, X. Wang and H. Wei, *Nat. commun.* 2023, 14, 3634.
- [5] J. Xu, S. Zhang, H. Liu, S. Liu, Y. Yuan, Y. Meng, M. Wang, C. Shen, Q. Peng and J. Chen, *Angew. Chem. Int. Ed.* 2023, 62, e202308044.
- [6] H. Wang, D. Zhao, C. Liu, X. Fan, Z. Li, Y. Luo, D. Zheng, S. Sun, J. Chen and J. Zhang, *Journal of Materials Chemistry A*, 2022, 10, 24462-24467.
- [7] X. Liu, X. Xu, F. Li, J. Xu, H. Ma, X. Sun, D. Wu, C. Zhang, X. Ren and Q. Wei, *ACS Applied Materials & Interfaces*, 2022, 14, 38835-38843.
- [8] N. Zhang, G. Zhang, Y. Tian, Y. Tang and K. Chu, *Dalton Transactions*, 2022, 51, 16805-16810.
- [9] J. Ye, A. Wang, M. Teng, Y. Yang, X. Qian, J. Xia, G. He and H. Chen, *Electrochimica Acta*, 2024, 482, 143985..
- [10] Y. Guo, R. Zhang, S. Zhang, Y. Zhao, Q. Yang, Z. Huang, B. Dong and C. Zhi, *Energy. Environ. Sci.* 2021, 14, 3938-3944.
- [11] R. Zhang, S. Zhang, Y. Guo, C. Li, J. Liu, Z. Huang, Y. Zhao, Y. Li and C. Zhi, *Energy. Environ. Sci.* 2022, 15, 3024-3032.
- [12] W. Luo, Z. Guo, L. Ye, S. Wu, Y. Jiang, P. Xu, H. Wang, J. Qian, X. Zhou and H. Tang, *Small*, 2024, 2311336.
- [13] Z. Chang, G. Meng, Y. Chen, C. Chen, S. Han, P. Wu, L. Zhu, H. Tian, F. Kong and M. Wang, *Adv. Mater.* 2023, 35, 2304508.
- [14] R. Zhang, Y. Guo, S. Zhang, D. Chen, Y. Zhao, Z. Huang, L. Ma, P. Li, Q. Yang and G. Liang, *Adv. Energy Mater.* 2022, 12, 2103872.